

# Orchid: Flexible and Data-Dependent Convolution for Sequence Modeling

Mahdi Karami<sup>1</sup> Ali Ghodsi<sup>1</sup>

## Abstract

In the rapidly evolving landscape of deep learning, the quest for models that balance expressivity with computational efficiency has never been more critical. This paper introduces Orchid, a novel architecture that reimagines sequence modeling by incorporating a new data-dependent convolution mechanism. Orchid is designed to address the inherent limitations of traditional attention mechanisms, particularly their quadratic complexity, without compromising the ability to capture long-range dependencies and in-context learning. At the core of Orchid lies the data-dependent convolution layer, which dynamically adjusts its kernel conditioned on input data using a dedicated conditioning neural network. We design two simple conditioning networks that maintain shift equivariance in the adaptive convolution operation. The dynamic nature of data-dependent convolution kernel, coupled with gating operations, grants Orchid high expressivity while maintaining efficiency and quasilinear scalability for long sequences. We rigorously evaluate Orchid across multiple domains, including language modeling and image classification, to showcase its performance and generality. Our experiments demonstrate that Orchid architecture not only outperforms traditional attention-based architectures such as BERT and Vision Transformers with smaller model sizes, but also extends the feasible sequence length beyond the limitations of the dense attention layers. This achievement represents a significant step towards more efficient and scalable deep learning models for sequence modeling.

## 1. Introduction

In the realm of modern deep neural networks, attention mechanisms have emerged as a gold standard, pivotal in domains such as natural language processing, image, and audio processing, and even complex fields like biology (Vaswani et al., 2017; Dosovitskiy et al., 2020; Dwivedi & Bresson, 2020). However, despite their strong sequence analysis capabilities, these mechanisms suffer from their high computational complexity, which scales quadratically with sequence length, hindering their application to long-context tasks. This complexity has driven a shift towards innovative solutions to overcome this computational barrier, enabling analysis of long sequences in areas like genomics, DNA sequencing, and the creation of long musical compositions.

Researchers have explored various strategies to tackle the computational bottleneck of traditional dense attention layers (Tay et al., 2022). One key strategy involves *sparsifying* the dense attention matrix. Instead of calculating the entire matrix, Qiu et al. (2019); Parmar et al. (2018) focus on specific local blocks of the receptive fields of sequences by chunking them into fixed-size blocks. Moreover, Sparse Transformer (Child et al., 2019), Longformer (Beltagy et al., 2020) and BigBird (Zaheer et al., 2020) use strided attention patterns combined with local sliding windows to reduce computation. In contrast to using pre-determined patterns, other techniques include learning to cluster/sort tokens based on a similarity function, thereby enhancing the global view of the sequence, as seen in Reformer (Kitaev et al., 2020), Routing Transformer (Roy et al., 2020) Sparse Sinkhorn attention (Tay et al., 2020). Another approach involves *low-rank approximations* of the self-attention matrix, leveraging the insight that these matrices often exhibit low-rank properties, as demonstrated by Linformer (Wang et al., 2020) which projects keys and values matrices to lower-dimensional representation matrices. Another paradigm to reduce quadratic computation cost, is to replace the dot-product similarity between keys and query matrices of attention mechanism with a *kernel function* and avoid explicitly computing the attention matrix (Katharopoulos et al., 2020). Notable examples in this family include Performers (Choromanski et al., 2020), Random Feature Attention (Peng et al., 2021) that are based on random feature approximation of the kernel function. Additionally, some models leverage a combinations of such techniques to de-

<sup>1</sup>School of Computer Science, University of Waterloo, ON, Canada. Correspondence to: Mahdi Karami <karami1@ualberta.ca>.

sign an efficient transformer (Zhu et al., 2021; Zhang et al., 2021). However, while these methods significantly reduce computational overhead, they may sacrifice expressiveness and performance, often requiring hybrid approaches that combine them with dense attention layers (Mehta et al., 2022; Fu et al., 2023b). On the other hand, recent works have aimed at sparsifying dense linear layers, used for feature mixing in Transformer blocks, to tackle another major source of high computation and memory demand in large models (Dao et al., 2022; Chen et al., 2021a;b).

Finding sub-quadratic and hardware-efficient mixing operators that are also expressive remains a significant challenge. Recent studies have explored attention-free solutions, particularly using state space models (SSMs) and long convolutions (Gu et al., 2021a; Romero et al., 2021; Mehta et al., 2022; Wang et al., 2022; Fu et al., 2023b; Poli et al., 2023). A state space model characterizes a dynamical system’s behavior in terms of its internal state using a state equation, describing the dynamics of the system using first-order differential equations over the states, and an observation equation, relating state variables to observed outputs.<sup>1</sup> A key insight is that SSMs can be formulated as a long convolution model between the input and output sequences (Gu et al., 2021b), allowing parallel and efficient training. However, recent work by Poli et al. (2023) demonstrated that directly parameterizing the filter impulse response of the long-convolution leads to an even more expressive sequence mixing layer.

This paper proposes a novel data-dependent convolution mechanism to tackle the inherent quadratic complexity of traditional attention mechanisms, while maintaining the model’s ability to capture long-range dependencies and in-context learning. The data-dependent convolution layer dynamically adjusts its kernel based on input data using a dedicated conditioning neural network. We design two simple yet effective conditioning networks that maintain shift equivariance in the adaptive convolution operation. By combining these adaptive mechanisms with gating operations, our proposed model—named *Orchid*—achieves high expressivity while offering quasilinear scalability (with a complexity of  $\mathcal{O}(L \log L)$ ) for long sequences.<sup>2</sup> Evaluation

<sup>1</sup>Notably, state space models, in general, include the recurrent layers such as RNN and LSTM (Hochreiter et al., 1997) as special cases.

<sup>2</sup>The name “*Orchid*” carries a symbolic meaning for our model, reflecting its elegance, resilience, and adaptability. Orchids are known to thrive in diverse environments and exhibit subtle color variations under specific environmental conditions, including light intensity, seasonal changes, and dyeing. The essence of adaptation and efficient resource utilization resonates profoundly with our model’s design. Moreover, the proposed model’s computational efficiency aligns with more environmentally sustainable AI practices by minimizing energy consumption and carbon footprint during training and deployment.

across various domains, including language modeling and image classification, demonstrates the Orchid architecture’s performance and generality, outperforming attention-based architectures, like BERT and Vision Transformers, with smaller model sizes. Moreover, its allows for handling very large sequence lengths that are beyond the limitations of the dense attention layers. This achievement lays the foundation for further advancements in more efficient and scalable sequence modeling architectures.

## 2. Background

**Self-Attention Mechanism:** Given a length- $L$  sequence of embeddings (of tokens)  $\mathbf{x} = (x_1, x_2, \dots, x_L)$ , self-attention generates a new sequence by computing a weighted sum of these embeddings. It does this by linearly projecting  $\mathbf{x}$  into three components: queries ( $\mathbf{Q}$ ), keys ( $\mathbf{K}$ ), and values ( $\mathbf{V}$ ), i.e.,

$$\mathbf{Q} = \mathbf{x}W^Q, \quad \mathbf{K} = \mathbf{x}W^K, \quad \mathbf{V} = \mathbf{x}W^V.$$

Each head of a self-attention (SA) can be expressed as a dense linear layer as follows:

$$\mathbf{y} = \text{SA}(\mathbf{Q}, \mathbf{K}, \mathbf{V}) = \text{SoftMax}\left(\frac{\mathbf{Q}\mathbf{K}^T}{\sqrt{d_k}}\right)\mathbf{V} = \mathbf{A}(\mathbf{x})\mathbf{V},$$

where the matrix  $\mathbf{A}(\mathbf{x})$  is populated with the attention scores between each pair of tokens. This description of the attention layer highlights its notable benefits, including its capability to capture long-range dependencies efficiently, with a sublinear parameter count. The attention mechanism enables direct computation of interactions between any two positions in the input sequence, regardless of their distance, without a corresponding rise in parameter counts. Additionally, the attention layer implements a *data-dependent* dense linear filter, effectively filtering the input while the filter weights are conditioned by a mapping of the data. This property makes it expressive and flexible enough to encode a large family of linear functions. However, these benefits come at the expense of quadratic computational complexity and memory costs.

This motivates us to develop an efficient and scalable *data-dependent convolution* mechanism, featuring a dynamic (adaptive) kernel that adjusts based on the input data. The kernel size of this convolution layer is as long as the input sequence length, allowing the capture of long-range dependencies across the input sequence while maintaining high scalability.

**Linear Convolution:** Discrete-time linear convolution is a fundamental operation in digital signal processing that calculates the output as the weighted sum of the finite-length input  $\mathbf{x}$  with shifted versions of the convolution kernel,  $\mathbf{h}$ ,

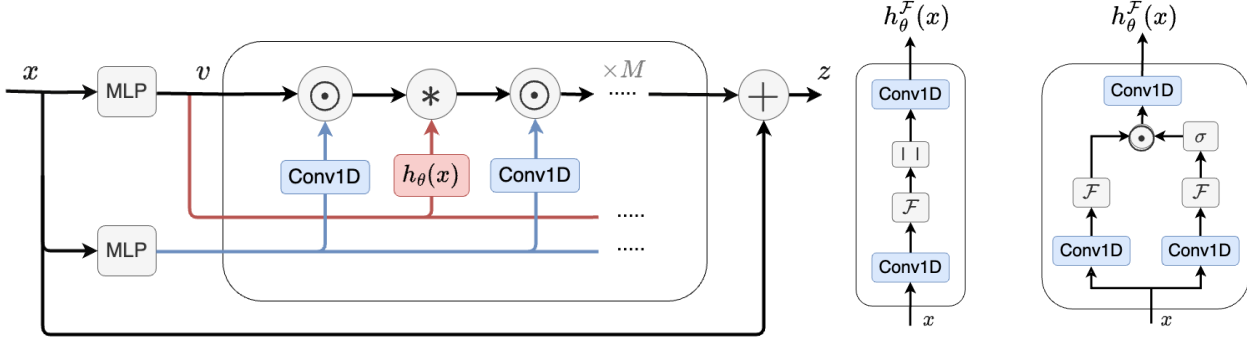


Figure 2.1: Orchid block.  $\odot$  and  $*$  denote element-wise multiplication and the convolution operator, respectively. The convolutions are implemented in the frequency domain using FFT. On the right two different conditioning networks, introduced in equations (2) and (3) as shift-invariant convolution kernels, are depicted.

also known as the impulse response of a linear time-invariant (LTI) system. Formally it can be written as

$$\mathbf{y}[t] = (\mathbf{h} * \mathbf{x})[t] \triangleq \sum_{\ell=0}^{L-1} h[t - \ell] x[\ell].$$

In this definition, the output is a linear filter of the *zero-padded* input and convolution kernel. However, other padding schemes leads to different forms of convolution. A well-known form is *circular convolution*, defined as

$$\mathbf{y}[t \bmod L] = (\mathbf{h} \circledast \mathbf{x})[t] \triangleq \sum_{\ell=0}^{L-1} h[t - \ell \bmod L] x[\ell],$$

which is equivalent to the linear convolution of two sequences when one is cyclically padded at its boundaries.

**Long Convolution and Fast Convolution Algorithm:** In standard convolution layers, the operation is explicitly parameterized with limited number of parameters. However, capturing long-range dependencies and correlations often requires a kernel as long as the input sequence, resulting in linear growth in parameter counts and also quadratic computational complexity. To address these challenges, firstly, we can retain sub-linear parameter scaling by implicitly parameterizing the convolution kernel with a multilayer perceptron (MLP) (Karami et al., 2019; Romero et al., 2021; Poli et al., 2023). On the other hand, one key advantage of convolution operators is that, according to the *convolution theorem*, they can be efficiently performed in the frequency domain using Fast Fourier Transform (FFT) algorithms (Cooley & Tukey, 1965) resulting in  $\mathcal{O}(L \log L)$  complexity. Formally, the linear convolution can be expressed as  $\hat{\mathbf{y}} = \mathcal{F}^{-1}(\mathcal{F}(\hat{\mathbf{h}}) \odot \mathcal{F}(\hat{\mathbf{x}})) = \mathbf{T}^{-1}(\mathbf{h}^{\mathcal{F}} \odot \mathbf{T}\hat{\mathbf{x}})$ , where  $\mathbf{T}$  is the DFT matrix,  $\mathcal{F}$  denotes the discrete Fourier transformation, and  $\hat{\mathbf{x}}$  denotes the zero-padded signal, defined as  $\hat{\mathbf{x}} \triangleq \text{pad}_{2L}(\mathbf{x}) = [\mathbf{0}_L; \mathbf{x}]$ . Additionally, the circu-

lar convolution can be simply computed as:  $\mathbf{y} = \mathbf{h} \circledast \mathbf{x} = \mathcal{F}^{-1}(\mathcal{F}(\mathbf{h}) \odot \mathcal{F}(\mathbf{x}))$ .<sup>3</sup>

### 3. Orchid

This section introduces the *Data-Dependent Convolution Filter*, a novel operator aimed at increasing the expressiveness of convolution operations. This operator serves as the foundational building block for the *Orchid* layer, which we will explore later in the section.

#### 3.1. Data-Dependent Convolution Filter

We hypothesize that making the convolutional kernel data-dependent allows the filter to adapt to the specific characteristics of its input, potentially capturing more complex patterns within the signal. Formally, the output of the filter is defined as:

$$\mathbf{y} = h_{\theta}(\mathbf{x}) * \mathbf{x} = \text{NN}_{\theta}(\mathbf{x}) * \mathbf{x} \quad (1)$$

<sup>3</sup>**Notation definition:** In this work, vectors, like  $\mathbf{x}$ , are represented by bold lowercase letters, while matrices are denoted by bold uppercase letters, such as  $\mathbf{W}$ . We differentiate between linear convolution ( $*$ ), circular convolution ( $\circledast$ ), cross-correlation ( $\star$ ), and element-wise multiplication ( $\odot$ ). The forward and inverse discrete Fourier transforms are denoted by  $\mathcal{F}$  and  $\mathcal{F}^{-1}$ , respectively, while The DFT matrix is represented by  $\mathbf{T}$ , and the *DFT* of a sequence  $\mathbf{x}$  is written as  $\mathbf{x}^{\mathcal{F}}$ .  $[\cdot]$  is used for indexing:  $\mathbf{x}^{\mathcal{F}}[\omega]$  represents the  $\omega$ th frequency component of sequence  $\mathbf{x}$ , while  $\mathbf{x}[t]$  refers to the value of  $\mathbf{x}$  at time  $t$ . Additionally, the data-dependent convolution kernel, also known as the *conditioning network*, is denoted by  $h_{\theta}(\mathbf{x}) = \text{NN}_{\theta}(\mathbf{x})$  that is a neural network parameterized by  $\theta$ . While generally  $\mathbf{x}$  represents a sequence of  $D$ -dimensional embeddings with length  $L$ , all the sequence mixing operators, including data-dependent convolutions, Fourier transforms and depthwise 1D convolutions (Conv1d) are performed along the sequence dimension. Therefore, for clarity and without loss of generality, we assume  $D = 1$  and  $\mathbf{x}$  is a vector in  $\mathbb{R}^L$ , unless explicitly stated otherwise.

The key innovation is to replace the static convolutional kernel with a dynamically generated one based on the input data. This is achieved through a *conditioning network*, denoted as  $h_\theta(\mathbf{x}) = \text{NN}_\theta(\mathbf{x})$ , parameterized by  $\theta$ . Since the conditioning network outputs a vector of the same length as the input sequence, each token in the input can "attend" to the entire signal with personalized weights learned based on the specific input representation. Convolving the surrounding context based on a data-dependent weighting scheme can potentially offer richer feature extraction compared to conventional static convolutional filters.

**Shift Equivariance of Convolution:** In general, a discrete convolution exhibits shift equivariance. This property implies that shifting the input by a specific amount results in the output shifting by the same amount (ignoring boundary effects). In circular convolution, this is formally expressed as:  $\text{shift}_m(\mathbf{y}) = \mathbf{h} \circledast \text{shift}_m(\mathbf{x})$  (Bronstein et al., 2021), where this property is true regardless of the boundary effects. Here,  $\text{shift}_m(\mathbf{x})[t]$  denotes the shift operation, defined as  $\text{shift}_m(\mathbf{x})[t] \triangleq \mathbf{x}[t + m]$ .

This property is particularly important because it ensures the operator's response is robust to shift of features within the input, thereby enhancing the model's generalization capabilities. This inductive bias is at the core of the widespread success of convolution operations (Thomas et al.). Therefore, it is desirable to design conditioning network in the data-dependent convolution (1) to preserve shift equivariance property. To maintain this property for convolution operations, it is sufficient to design filter kernel to be *shift invariant*. In the following, we present two shift-invariant conditioning networks.

**I) Suppressing the Phase of Frequency Components:** A circular shift of a sequence  $\mathbf{u}$  amounts to multiplying its frequency components by a linear phase factor:  $\mathcal{F}(\text{shift}_m(\mathbf{u}))[\omega] = \mathbf{u}^{\mathcal{F}}[\omega] \cdot e^{-\frac{i2\pi}{L}\omega m}$  (Oppenheim, 1999). Consider a function  $g(\mathbf{x})$  that's shift-equivariant (such as a depthwise `Conv1d()`):  $g(\text{shift}_m(\mathbf{x})) = \text{shift}_m(g(\mathbf{x}))$ . Its frequency components after a spatial shift of its input can be expressed as:

$$\mathcal{F}(g(\text{shift}_m(\mathbf{x})))[\omega] = \mathcal{F}(g(\mathbf{x}))[\omega] \cdot e^{-\frac{i2\pi}{L}\omega m}.$$

By taking the magnitude (absolute value or squared) of these complex-valued frequency components, we eliminate the phase shift and achieve shift invariance. Hence, defining  $h^{\mathcal{F}}(\mathbf{x}) = |\mathcal{F}(g(\mathbf{x}))|$  satisfies shift invariance:  $h^{\mathcal{F}}(\text{shift}_m(\mathbf{x})) = h^{\mathcal{F}}(\mathbf{x})$ .

In our setup, we utilize a 1D depthwise linear convolution (`Conv1d()`) with a short kernel length (typically 3-5) applied separately to each feature dimension. This is followed by a short convolution in the frequency domain. Conse-

quently, the conditioning neural network is formulated as

$$h_\theta^{\mathcal{F}}(\mathbf{x}) = \text{Conv1d}(|\mathcal{F}(\text{Conv1d}(\mathbf{x}))|) \quad (2)$$

This architecture choice aims to minimize the number of parameters and computational burden introduced by the conditioning network within the overall model.

## II) Using Cross-Correlation to Achieve Shift Invariance

An alternative method for achieving shift invariance involves computing the cross-correlation between two versions of a signal. Consider  $k(\mathbf{x})$  and  $q(\mathbf{x})$  as two shift-equivariant functions, satisfying:  $k(\text{shift}_m(\mathbf{x})) = \text{shift}_m(k(\mathbf{x}))$  and  $q(\text{shift}_m(\mathbf{x})) = \text{shift}_m(q(\mathbf{x}))$ . Define  $h(\mathbf{x})$  as the cross-correlation of  $k(\mathbf{x})$  and  $q(\mathbf{x})$ , given by:

$$h(\mathbf{x})[t] = (k(\mathbf{x}) \star q(\mathbf{x}))[t] \triangleq \sum_{\ell=0}^{L-1} k(\mathbf{x})[\ell] \cdot q(\mathbf{x})[t + \ell \bmod L].$$

This operation essentially slides  $q(\mathbf{x})$  over  $k(\mathbf{x})$  and measures their similarity at different offsets. Remarkably, this cross-correlation function,  $h(\mathbf{x})$ , is also shift invariant:

$$\begin{aligned} h(\text{shift}_m(\mathbf{x})) &= k(\text{shift}_m(\mathbf{x})) \star q(\text{shift}_m(\mathbf{x})) \\ &= \text{shift}_m(k(\mathbf{x})) \star \text{shift}_m(q(\mathbf{x})) \\ &= k(\mathbf{x}) \star q(\mathbf{x}) = h(\mathbf{x}) \end{aligned}$$

Furthermore, the convolution theorem allows us to efficiently compute the cross-correlation in the frequency domain:  $h^{\mathcal{F}}(\mathbf{x}) = \mathcal{F}(k(\mathbf{x}) \star q(\mathbf{x})) = k^{\mathcal{F}^*}(\mathbf{x}) \odot q^{\mathcal{F}}(\mathbf{x})$  where  $k^{\mathcal{F}^*}$  denotes the complex conjugate of  $k^{\mathcal{F}}$  and  $\odot$  represents element-wise multiplication.

*Remark 3.1.* By setting  $k(\mathbf{x}) = q(\mathbf{x}) = g(\mathbf{x})$ , we derive  $h^{\mathcal{F}}(\mathbf{x}) = |g^{\mathcal{F}}(\mathbf{x})|^2$ . This implies that the cross-correlation approach generalizes the magnitude-based approach, demonstrating its versatility.

Similar to the previous approach, we utilize distinct 1D depth-wise short convolutions for both  $k(\mathbf{x})$  and  $q(\mathbf{x})$ , followed by another convolution post cross-correlation in the frequency domain. As a result, the conditioning neural network is defined as

$$\begin{aligned} h_\theta^{\mathcal{F}}(\mathbf{x}) &= \text{Conv1d} \left( \mathcal{F}^*(\text{Conv1d}(\mathbf{x})) \odot \sigma(\mathcal{F}(\text{Conv1d}(\mathbf{x}))) \right). \end{aligned} \quad (3)$$

Inspired by gating mechanism, we applied  $\sigma() = \text{Sigmoid}()$  to one of the sequences in the frequency domain. Both conditioning functions, described in equations 2 and 3, are also schematically visualized in Figure 2.1.

*Remark 3.2.* For convolution operations, we augment the data-dependent conditioning network with a fixed (non dynamic) term. This term adds positional encoding to the convolution kernel by implicitly parametrizing it using a

positional embedding ( $\text{PosEmb}()$ ) of time step (token index in the sequence) and a feed forward networks ( $\text{FFN}()$ )  $h(t) = \text{FFN}(\text{PosEmb}(t))$  (Romero et al., 2021).

Finally, the combined convolution kernel is obtained by  $h = h(t) + h_\theta(x)$ .

### 3.2. Orchid Block

Unlike attention layers, convolution filters leverage parameter sharing, This means they slides the same kernel weights and apply them to different positions within the input sequence. Mathematically, this operation can be represented as multiplying an input vector with a structured matrix, like a Toeplitz matrix for linear convolutions or a circulant matrix for circular convolutions, resulting in computational efficiency (Gray et al., 2006; Karami et al., 2019). To achieve a location-dependent filtering scheme, we complement the (data-dependent) convolution with element-wise multiplications. This allows us to emphasize specific locations within the signal by assigning higher weights before applying the location-invariant convolution. Notably, studies have shown that a cascade of circulant and diagonal matrices can efficiently approximate dense linear layers (Moczulski et al., 2015; Cheng et al., 2015). Leveraging these insights, the overall architecture of the Orchid block, composed of a chain of  $M$  data-dependent convolution and element-wise multiplications, is illustrated in Figure 2.1.

**Overall Computational complexity:** All long convolutions are performed in the frequency domain using FFT algorithm hence inheriting its computational efficiency for sequence mixing, with a time complexity of  $\mathcal{O}(L \log L)$ . Additionally, element-wise multiplications contribute an  $\mathcal{O}(L)$  complexity. Hence, considering the entire block, the overall complexity of the Orchid block scales quasilinearly with the sequence length, resulting in an overall complexity of  $\mathcal{O}(ML \log L)$ .

**Remark 3.3 (data-dependent Convolution as a Cross-attention Alternative).** The kernel of convolution  $h_\theta(x)$ , defined in equations (2) or (3), is conditioned the input of the convolution layer, making it input-dependent. However, convolution kernel can generally be a functions of an arbitrary sequence  $u$ , leading to the generalized form of data-dependent convolution:

$$y(x, u) = h_\theta(u) * x = \text{NN}_\theta(u) * x$$

This definition couples the input signal  $x$  with another signal  $u$ , creating a potential alternative to cross-attention layers. We therefore refer to the proposed layer as "data-dependent" in a general sense. When dealing with signals of different lengths, the shorter one can be zero-padded to match the length of the longer one. Specifically, assuming  $x \in \mathbb{R}^L$  is longer than  $u \in \mathbb{R}^N$  ( $L > N$ ), we use the zero-padded signal  $\hat{u} = \text{pad}_L(u) \in \mathbb{R}^L$  as input to the conditioning network

$\text{NN}_\theta(\hat{u})$ . Since the long convolution is implemented in the frequency domain, this zero-padding in the time domain corresponds to interpolation in the frequency domain (Smith, 2008) ensuring that both signals have frequency components of the same size.

## 4. Experiments

Our evaluation of Orchid focuses on three different Transformer-based models to assess its expressivity and generalization capabilities as an alternative to attention layers. Firstly, we conduct a set of experiments on a synthetic task to assess the in-context learning ability and scalability of the proposed model. Subsequently, we evaluate the performance of the proposed architecture on language modeling tasks. Moreover, we extend our experiments to image classification tasks, aiming to evaluate the model's generalizability across diverse domains.

### 4.1. Synthetic In-context Learning

The aim of the first experiment is to assess how well our model performs on a synthetic reasoning task. This task, inspired by prior work on language model benchmarking (Liang et al., 2022) and in-context learning (ICL) (Garg et al., 2022), is known as Associative Recall. It involves generating a value from a key given a string of key-value tuples from a random dictionary. For instance, given the input  $([a, 1, b, e, \beta, f], b)$ , the model is expected to return  $e$ , the value associated with the key  $b$ . This task assesses whether a model can effectively retrieve the correct value from a key in a prompt, essentially applying a data-controlled shift. Attention mechanisms offer this capability by computing attention scores through token comparisons and then weighting the entire sequence accordingly (Olsson et al., 2022). Associative recall has been pivotal in guiding the design of long convolution models, as demonstrated in (Fu et al., 2023b), and a more complex variant of this task was employed in (Poli et al., 2023) to benchmark Hyena.

For these experiments, we benchmark Orchid against several leading long convolution models, including:

- H3: Utilizes state-space models (SSMs) for implicit parametrization of long convolution, as proposed in (Fu et al., 2023b).
- CKConv: Employs feedforward networks (FFNs) and positional embeddings for the implicit parametrization of convolution operations, detailed in (Romero et al., 2021).
- Hyena: Builds upon the CKConv framework by incorporating an additional exponential decay modulation into the implicit convolution process, as detailed in

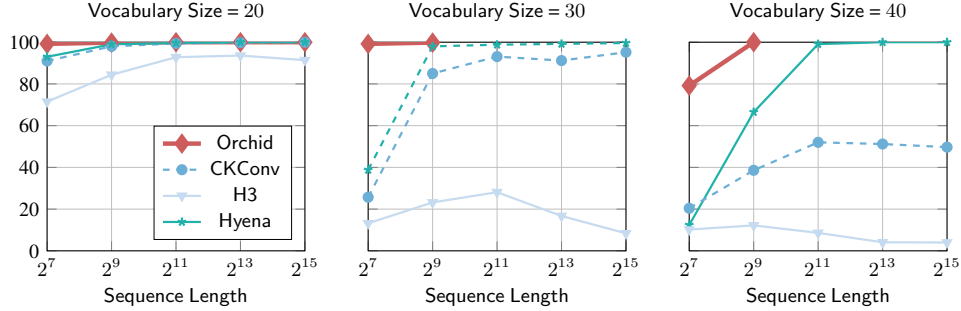


Figure 3.1: Performance of the associative recall task across different long implicit convolution models on various sequence lengths and vocabulary sizes (number of possible token values).

Table 4.1: This table shows the performance of in-context learning on the associative recall task with a vocabulary size of 20 and different sequence lengths. The results for the baseline models are drawn from (Poli et al., 2023; Fu et al., 2023a). The symbol  $\times$  indicates that the Transformer model failed to complete the task within a week or the model does not fit in memory.

Model	128	512	2K	8K	32K	128K
Transformer	100	100	100	100	$\times$	$\times$
Monarch-Mixer	-	98.7	99.4	99.4	99.4	99.4
Hyena	93	99	99.6	100	100	-
Orchid	99.2	99.8	100	100	100	100

(Poli et al., 2023). It is further augmented by a multiplication mechanism in a chain of order 2.

The results, illustrated in Figure 3.1 and Table 4.1, demonstrate that the Orchid model offers superior expressiveness and outperforms existing long convolution models in the associative recall task. Notably, in challenging scenarios with short sequence lengths of 128 and large vocabulary sizes, Orchid significantly improves the model’s accuracy and narrows the gap between Transformer and implicit convolution models. Furthermore, when extending the sequence length to very long sequences of up to 131K, Orchid demonstrates successful task learning while the Transformer model encounters computational difficulties.

The insights from this experiment guide us in integrating the proposed model into Transformer-based models for extensive language modeling, suggesting its potential to enhance performance in natural language processing tasks.

## 4.2. Language Modeling

We evaluate the Orchid layer in language models. Orchid is designed to integrate seamlessly with existing BERT-style language models, such as BERT (Devlin et al., 2018), RoBERTa (Liu et al., 2019), SpanBERT (Joshi et al., 2020),

and others (Jin et al., 2020). In our experiments, we replace the attention layers in the standard BERT framework in (Devlin et al., 2018) with Orchid layers. For each Transformer block in the BERT-style model, we replace the attention layers with Orchid layers for sequence mixing. We also replace the two dense matrices in the MLP layers with block-diagonal matrices (Dao et al., 2022) for dimension mixing. Following (Fu et al., 2023a), we add a residual long convolution to each Orchid layer.

Our BERT-style model, called Orchid-BERT-base, has 12 layers with a hidden size of 768, the same dimension and depth as BERT-base. This results in Orchid-BERT-base having 77M parameters, compared to BERT-base’s 110M parameters. We also pretrain Orchid-BERT-large of 254M parameters with hidden dimensions of 1536 and 12 layers. Orchid models are pre-trained using masked language modeling over the C4 dataset (Raffel et al., 2019) with the bert-base-uncased tokenizer.

**Finetuning Performance on GLUE Benchmark** We conducted an evaluation of Orchid-BERT models on GLUE fine-tuning tasks, comparing them against the baseline models: BERT-base and BERT-large, and the recent long convolution-based models: M2-BERT-base and M2-BERT-large (Fu et al., 2023a). The fine-tuning process was executed in accordance with the methodology described by Izsak et al. (2021). As the results outlined in Table 4.2 show, Orchid-BERT-base is able to achieve 1.0 points improvement in average GLUE score performance compared to the BERT-base on the GLUE benchmark with utilizing 30% fewer parameters. Similarly, Orchid-BERT-large outperforms the performance of BERT-large by .6 points with a 25% reduction in parameter counts.

## 4.3. Image Classification

We extend the application of Orchid to the Vision Transformer (ViT) architecture, introduced by Dosovitskiy et al. (2020), by replacing its attention mechanism with Orchid

Table 4.2: Average GLUE Score of BERT-base and BERT-large (Devlin et al., 2018) in comparison to Orchid-BERT-base and Orchid-BERT-base, and M2-BERT-base and M2-BERT-large (Dao et al., 2022). Baseline results are drawn from (Fu et al., 2023a).

Model (size)	GLUE Score	$\Delta$ Params	$\Delta$ GLUE Score
BERT-base (110M)	79.6	-	-
M2-BERT-base (80M)	79.9	-27.3%	+0.3
Orchid-BERT-base (77M)	<b>80.6</b>	<b>-30.0%</b>	+1.0
BERT-large (340M)	82.1	-	-
M2-BERT-large (260M)	82.2	-23.6%	+0.1
Orchid-BERT-large (254M)	<b>82.7</b>	<b>-25.3%</b>	+0.6

Table 4.3: Performance comparison of Orchid with ViT-based models on ImageNet-1k and CIFAR-10 dataset. Baseline results are drawn from (Fu et al., 2023a).

Model (size)	Top-1 (%)	Top-5 (%)	Model (size)	Top-1 (%)
<i>ImageNet-1k</i>				
ViT-b (87M)	78.5	93.6	ViT (1.2M)	78.6
ViT-b + Monarch (33M)	78.9	94.2	ViT + Monarch (607K)	79.0
Hyena-ViT-b (88M)	78.5	93.6	Hyena-ViT (1.3M)	80.6
M2-ViT-b (45M)	79.5	94.5	M2-ViT (741K)	80.8
Orchid-ViT-b (48M)	<b>80.2</b>	<b>94.9</b>	Orchid-ViT (836K)	<b>84.3</b>
<i>CIFAR-10</i>				

similar to language modeling task. Additionally, we substitute the dense matrices in the MLP layers, which perform dimension mixing, with block-diagonal matrices and incorporate a residual long convolution within each Orchid block. We benchmark our model against recent long convolution-based models, specifically Hyena-ViT-b (Poli et al., 2023) and M2-ViT-b (Fu et al., 2023a).

Models are evaluated for image classification on two widely used image datasets: CIFAR-10 and ImageNet-1K. For CIFAR-10, images are transformed into sequences of  $4 \times 4$  pixel patches and processed using a ViT architecture composed of 6 Transformer layers with a hidden size of 128. In the case of ImageNet-1K, we segmented images into patches of  $16 \times 16$  pixels, and we trained a ViT-base architecture featuring 12 Transformer layers and a hidden size of 768.

The models’ performance on both the CIFAR-10 and ImageNet-1K datasets, outlined in Table 4.3, demonstrate that Orchid significantly outperforms both the Vision Transformer baseline and the long convolution-based models on both datasets. These results affirm the generalizability and effectiveness of the Orchid architecture beyond the domain of language modeling, highlighting its potential advantage in broader range of applications such as image processing tasks.

## 5. Related Work

Recent studies have explored sub-quadratic sequence mixing methods using long convolutions or state space models, leveraging the fast convolution algorithm for computational efficiency. While utilizing Fast Fourier transform results in  $\mathcal{O}(L \log L)$  computational complexity, FFT algorithms exhibit suboptimal hardware utilization and suffer from slow I/O between layers of the memory hierarchy on modern GPUs due to their sequential nature. To address this bottleneck, FlashFFTConv (Fu et al., 2023c) introduced a more hardware and I/O efficient implementation of long convolutions. This approach utilizes matrix decomposition to leverage matrix multiply units and enable kernel fusion, resulting in significant speedup on modern parallel processing units.

More recently, the Monarch Mixer (M2) (Fu et al., 2023a), offers an expressive family of sub-quadratic structured matrices that generalizes the DFT and other structures. These matrices are parameterized as products of block-diagonal matrices, offering sub-quadratic computation costs ranging from  $\mathcal{O}(L \log L)$  to  $\mathcal{O}(L^{3/2})$ . By trading-off computational complexity with FLOP utilization, M2 achieves a hardware-efficient alternative for Transformers.

## 6. Discussion and Conclusion

In conclusion, our work introduces Orchid, a groundbreaking model that addresses some critical challenges of efficiency and scalability in sequence modeling through the innovative use of data-dependent convolution. Orchid successfully mitigates the quadratic computational and memory costs associated with them, while retaining, and in many cases enhancing, the model performance across different domains. The introduction of a data-dependent convolution layer represents a significant step forward, offering a scalable and expressive alternative filtration scheme that adapts its weights to the input data. Through evaluation across multiple domains, including language and image processing tasks, Orchid has demonstrated not only its superior performance over traditional attention-based models but also its generality and scalability. This positions the Orchid model not just as a competitor to existing paradigms but as a catalyst for innovation, driving the exploration of novel, efficient, and powerful architectures in the realm of artificial intelligence.

The remarkable performance of our model when compared to traditional transformer-based models raises pertinent questions about the current state and future direction of deep learning architectures. One plausible reason for our model's superiority could be the over-parameterization prevalent in contemporary models. This suggests that there might exist far more efficient architectures yet to be explored. A growing body of evidence indicates that attention mechanisms, despite their computational complexity, utilize only a fraction of their capabilities for tasks like language processing. This finding challenges the common belief that attention is the key ingredient for large-scale deep learning, leading us to reconsider its role and seek more computationally efficient alternatives.

Looking ahead, extending our model to accommodate causal models, particularly for autoregressive language models akin to GPT, is an intriguing future direction. The current version of our model is not inherently aligned with such architectures, primarily due to differences in how they handle dependencies and sequence generation. Furthermore, adapting our model to sequence-to-sequence models and incorporating cross-attention mechanisms present additional avenues for exploration and enhancement. These considerations open up new possibilities for integrating our model into more complex language generation tasks and cross-domain applications.

## 7. Broader Impacts

The introduction of Orchid, with its innovative data-dependent convolution mechanism, marks a significant advancement in the field of deep learning, potentially leading to far-reaching impacts across various sectors of society.

- **Accessibility and Democratization of AI:** By reducing the computational and memory requirements traditionally associated with deep learning models, Orchid makes advanced AI technologies more accessible to a broader range of researchers, startups, and institutions.
- **Environmental Sustainability:** The efficiency of Orchid, particularly in terms of computational and energy demands, aligns with the urgent need for environmentally sustainable AI practices. Lower energy consumption contributes to reducing the carbon footprint of training and deploying large-scale models, aligning with global sustainability goals.
- **Advancements in Healthcare:** In the healthcare sector, Orchid's ability to efficiently process long sequences of data could revolutionize early diagnosis and personalized medicine. For instance, it could enable more accurate analysis of genomic sequences or continuous health monitoring data, leading to earlier detection of diseases and tailored treatment plans.

## References

Beltagy, I., Peters, M. E., and Cohan, A. Longformer: The long-document transformer. *arXiv preprint arXiv:2004.05150*, 2020.

Beyer, L., Zhai, X., and Kolesnikov, A. Better plain ViT baselines for imagenet-1k. *arXiv preprint arXiv:2205.01580*, 2022.

Bronstein, M. M., Bruna, J., Cohen, T., and Veličković, P. Geometric deep learning: Grids, groups, graphs, geodesics, and gauges. *arXiv preprint arXiv:2104.13478*, 2021.

Chen, B., Dao, T., Liang, K., Yang, J., Song, Z., Rudra, A., and Ré, C. Pixelated butterfly: Simple and efficient sparse training for neural network models. 2021a.

Chen, B., Dao, T., Winsor, E., Song, Z., Rudra, A., and Ré, C. Scatterbrain: Unifying sparse and low-rank attention. In *Advances in Neural Information Processing Systems (NeurIPS)*, 2021b.

Cheng, Y., Yu, F. X., Feris, R. S., Kumar, S., Choudhary, A., and Chang, S.-F. An exploration of parameter redundancy in deep networks with circulant projections. In *Proceedings of the IEEE International Conference on Computer Vision*, pp. 2857–2865, 2015.

Child, R., Gray, S., Radford, A., and Sutskever, I. Generating long sequences with sparse transformers. *arXiv preprint arXiv:1904.10509*, 2019.

Choromanski, K., Likhoshesterov, V., Dohan, D., Song, X., Gane, A., Sarlos, T., Hawkins, P., Davis, J., Mohiuddin, A., Kaiser, L., et al. Rethinking attention with performers. *arXiv preprint arXiv:2009.14794*, 2020.

Cooley, J. W. and Tukey, J. W. An algorithm for the machine calculation of complex fourier series. *Mathematics of computation*, 19(90):297–301, 1965.

Dao, T., Chen, B., Sohoni, N. S., Desai, A., Poli, M., Grogan, J., Liu, A., Rao, A., Rudra, A., and Ré, C. Monarch: Expressive structured matrices for efficient and accurate training. In *International Conference on Machine Learning*. PMLR, 2022.

Devlin, J., Chang, M.-W., Lee, K., and Toutanova, K. BERT: Pre-training of deep bidirectional transformers for language understanding. *arXiv preprint arXiv:1810.04805*, 2018.

Dosovitskiy, A., Beyer, L., Kolesnikov, A., Weissenborn, D., Zhai, X., Unterthiner, T., Dehghani, M., Minderer, M., Heigold, G., Gelly, S., et al. An image is worth 16x16 words: Transformers for image recognition at scale. *arXiv preprint arXiv:2010.11929*, 2020.

Dwivedi, V. P. and Bresson, X. A generalization of transformer networks to graphs. *arXiv preprint arXiv:2012.09699*, 2020.

Fu, D. Y., Arora, S., Grogan, J., Johnson, I., Eyuboglu, S., Thomas, A. W., Spector, B., Poli, M., Rudra, A., and Ré, C. Monarch mixer: A simple sub-quadratic gemm-based architecture. *arXiv preprint arXiv:2310.12109*, 2023a.

Fu, D. Y., Dao, T., Saab, K. K., Thomas, A. W., Rudra, A., and Ré, C. Hungry hungry hippos: Towards language modeling with state space models. *International Conference on Learning Representations*, 2023b.

Fu, D. Y., Kumbong, H., Nguyen, E., and Ré, C. Flashfftconv: Efficient convolutions for long sequences with tensor cores. *arXiv preprint arXiv:2311.05908*, 2023c.

Garg, S., Tsipras, D., Liang, P., and Valiant, G. What can transformers learn in-context? a case study of simple function classes. *arXiv preprint arXiv:2208.01066*, 2022.

Gray, R. M. et al. Toeplitz and circulant matrices: A review. *Foundations and Trends® in Communications and Information Theory*, 2(3):155–239, 2006.

Gu, A., Goel, K., and Ré, C. Efficiently modeling long sequences with structured state spaces. *arXiv preprint arXiv:2111.00396*, 2021a.

Gu, A., Johnson, I., Goel, K., Saab, K., Dao, T., Rudra, A., and Ré, C. Combining recurrent, convolutional, and continuous-time models with linear state space layers. *Advances in neural information processing systems*, 34: 572–585, 2021b.

Hochreiter, S., Schmidhuber, J., et al. Long short-term memory. *Neural computation*, 9(8):1735–1780, 1997.

Izsak, P., Berchansky, M., and Levy, O. How to train BERT with an academic budget. In *Proceedings of the 2021 Conference on Empirical Methods in Natural Language Processing*, pp. 10644–10652, 2021.

Jin, D., Jin, Z., Zhou, J. T., and Szolovits, P. Is BERT really robust? a strong baseline for natural language attack on text classification and entailment. In *Proceedings of the AAAI conference on artificial intelligence*, volume 34, pp. 8018–8025, 2020.

Joshi, M., Chen, D., Liu, Y., Weld, D. S., Zettlemoyer, L., and Levy, O. Spanbert: Improving pre-training by representing and predicting spans. *Transactions of the Association for Computational Linguistics*, 8:64–77, 2020.

Karami, M., Schuurmans, D., Sohl-Dickstein, J., Dinh, L., and Duckworth, D. Invertible convolutional flow. *Advances in Neural Information Processing Systems*, 32, 2019.

Katharopoulos, A., Vyas, A., Pappas, N., and Fleuret, F. Transformers are rnns: Fast autoregressive transformers with linear attention. In *International Conference on Machine Learning*, pp. 5156–5165. PMLR, 2020.

Kingma, D. P. and Ba, J. Adam: A method for stochastic optimization. *arXiv preprint arXiv:1412.6980*, 2014.

Kitaev, N., Kaiser, L., and Levskaya, A. Reformer: The efficient transformer. In *International Conference on Learning Representations*, 2020.

Liang, P., Bommasani, R., Lee, T., Tsipras, D., Soylu, D., Yasunaga, M., Zhang, Y., Narayanan, D., Wu, Y., Kumar, A., et al. Holistic evaluation of language models. *arXiv preprint arXiv:2211.09110*, 2022.

Liu, Y., Ott, M., Goyal, N., Du, J., Joshi, M., Chen, D., Levy, O., Lewis, M., Zettlemoyer, L., and Stoyanov, V. Roberta: A robustly optimized BERT pretraining approach. *arXiv preprint arXiv:1907.11692*, 2019.

Mehta, H., Gupta, A., Cutkosky, A., and Neyshabur, B. Long range language modeling via gated state spaces. *arXiv preprint arXiv:2206.13947*, 2022.

Moczulski, M., Denil, M., Appleyard, J., and de Freitas, N. Acdc: A structured efficient linear layer. *arXiv preprint arXiv:1511.05946*, 2015.

Olsson, C., Elhage, N., Nanda, N., Joseph, N., DasSarma, N., Henighan, T., Mann, B., Askell, A., Bai, Y., Chen, A., Conerly, T., Drain, D., Ganguli, D., Hatfield-Dodds, Z., Hernandez, D., Johnston, S., Jones, A., Kernion, J., Lovitt, L., Ndousse, K., Amodei, D., Brown, T., Clark, J., Kaplan, J., McCandlish, S., and Olah, C. In-context learning and induction heads. *Transformer Circuits Thread*, 2022. <https://transformer-circuits.pub/2022/in-context-learning-and-induction-heads/index.html>.

Oppenheim, A. V. *Discrete-time signal processing*. Pearson Education India, 1999.

Parmar, N., Vaswani, A., Uszkoreit, J., Kaiser, L., Shazeer, N., Ku, A., and Tran, D. Image transformer. *Proceedings of ICML 2018*, 2018.

Peng, H., Pappas, N., Yogatama, D., Schwartz, R., Smith, N. A., and Kong, L. Random feature attention. *Proceedings of ICLR*, 2021.

Poli, M., Massaroli, S., Nguyen, E., Fu, D. Y., Dao, T., Baccus, S., Bengio, Y., Ermon, S., and Ré, C. Hyena hierarchy: Towards larger convolutional language models. *International Conference on Machine Learning*, 2023.

Qiu, J., Ma, H., Levy, O., Yih, S. W.-t., Wang, S., and Tang, J. Blockwise self-attention for long document understanding. *arXiv preprint arXiv:1911.02972*, 2019.

Raffel, C., Shazeer, N., Roberts, A., Lee, K., Narang, S., Matena, M., Zhou, Y., Li, W., and Liu, P. J. Exploring the limits of transfer learning with a unified text-to-text transformer. *arXiv preprint arXiv:1910.10683*, 2019.

Romero, D. W., Kuzina, A., Bekkers, E. J., Tomczak, J. M., and Hoogendoorn, M. Ckconv: Continuous kernel convolution for sequential data. In *International Conference on Learning Representations*, 2021.

Roy, A., Saffar, M., Vaswani, A., and Grangier, D. Efficient content-based sparse attention with routing transformers. *Proceedings of TACL*, 2020.

Smith, J. O. *Mathematics of the discrete Fourier transform (DFT): with audio applications*. Julius Smith, 2008.

Steiner, A., Kolesnikov, A., Zhai, X., Wightman, R., Uszkoreit, J., and Beyer, L. How to train your ViT? data, augmentation, and regularization in vision transformers. *arXiv preprint arXiv:2106.10270*, 2021.

Tay, Y., Bahri, D., Yang, L., Metzler, D., and Juan, D.-C. Sparse sinkhorn attention. *Proceedings of ICML*, 2020.

Tay, Y., Dehghani, M., Bahri, D., and Metzler, D. Efficient transformers: A survey. *ACM Computing Surveys*, 55(6): 1–28, 2022.

Thomas, N., Smidt, T., Kearnes, S., Yang, L., Li, L., Kohlhoff, K., and Riley, P. Tensor field networks: Rotation-and translation-equivariant neural networks for 3d point clouds. arxiv 2018. *arXiv preprint arXiv:1802.08219*.

Vaswani, A., Shazeer, N., Parmar, N., Uszkoreit, J., Jones, L., Gomez, A. N., Kaiser, L., and Polosukhin, I. Attention is all you need. volume 30, 2017.

Wang, A., Singh, A., Michael, J., Hill, F., Levy, O., and Bowman, S. R. Glue: A multi-task benchmark and analysis platform for natural language understanding. *arXiv:1804.07461*, 2018.

Wang, J., Yan, J. N., Gu, A., and Rush, A. M. Pretraining without attention. *arXiv preprint arXiv:2212.10544*, 2022.

Wang, S., Li, B. Z., Khabsa, M., Fang, H., and Ma, H. Linformer: Self-attention with linear complexity. *arXiv preprint arXiv:2006.04768*, 2020.

Yuan, L., Chen, Y., Wang, T., Yu, W., Shi, Y., Jiang, Z.-H., Tay, F. E., Feng, J., and Yan, S. Tokens-to-token ViT: Training vision transformers from scratch on imagenet. In *Proceedings of the IEEE/CVF international conference on computer vision*, pp. 558–567, 2021.

Zaheer, M., Guruganesh, G., Dubey, A., Ainslie, J., Alberti, C., Ontanon, S., Pham, P., Ravula, A., Wang, Q., Yang, L., et al. Big bird: Transformers for longer sequences. *Proceedings of NeurIPS*, 2020.

Zhang, H., Gong, Y., Shen, Y., Li, W., Lv, J., Duan, N., and Chen, W. Poolingformer: Long document modeling with pooling attention. *Proceedings of ICML*, 2021.

Zhu, C., Ping, W., Xiao, C., Shoeybi, M., Goldstein, T., Anandkumar, A., and Catanzaro, B. Long-short transformer: Efficient transformers for language and vision. *Advances in Neural Information Processing Systems*, 34: 17723–17736, 2021.

## A. Notation definition

Notations	Brief definition and interpretation
$\mathbf{x}, \mathbf{y}, \mathbf{W}$	$\mathbf{x} \in \mathbb{R}^L$ and $\mathbf{y} \in \mathbb{R}^L$ are input and output sequence of a layer, while matrices are denoted by bold uppercase letters, such as layer weight matrix $\mathbf{W}$ .
$\mathbf{h} * \mathbf{x}$	linear convolution: $\mathbf{y}[t] = (\mathbf{h} * \mathbf{x})[t] \triangleq \sum_{\ell=0}^{L-1} h[t - \ell]x[\ell]$
$\mathbf{h} \circledast \mathbf{x}$	circular convolution: $\mathbf{y}[t \bmod L] = (\mathbf{h} \circledast \mathbf{x})[t] \triangleq \sum_{\ell=0}^{L-1} h[t - \ell \bmod L]x[\ell]$
$\mathbf{k} \star \mathbf{q}$	cross-correlation: $\mathbf{h}[t] = (\mathbf{k} \star \mathbf{q})[t] \triangleq \sum_{\ell=0}^{L-1} \mathbf{k}[\ell] \cdot \mathbf{q}[t + \ell \bmod L]$
$\mathbf{h} \odot \mathbf{x}$	element-wise multiplication (Hadamard product): $\mathbf{y}[t] = (\mathbf{h} \odot \mathbf{x})[t] \triangleq h[t] \cdot x[t]$
$\text{shift}_m(\mathbf{x})$	$\text{shift}_m(\mathbf{x})[t] \triangleq \mathbf{x}[t + m]$
$\mathcal{F}(), \mathcal{F}^{-1}(), \mathbf{T}$	The forward and inverse discrete Fourier transforms while $\mathbf{T}$ represents the DFT matrix.
$\mathbf{x}^{\mathcal{F}}$	$\mathbf{x}^{\mathcal{F}} = \mathcal{F}(\mathbf{x}) = \mathbf{T}\mathbf{x}$
$\hat{\mathbf{x}}$	$\hat{\mathbf{x}} \in \mathbb{R}^{2L}$ is a zero-padded signal at the left side defined as $\hat{\mathbf{x}} \triangleq \text{pad}_{2L}(\mathbf{x}) = [\mathbf{0}_L; \mathbf{x}]$
$\text{pad}_N(\mathbf{x})$	padding the vector $\mathbf{x} \in \mathbb{R}^L$ with zeros to the target size $N$ , i.e. $\text{pad}_N(\mathbf{x}) = [\mathbf{0}_{N-L}; \mathbf{x}]$ where $[\mathbf{0}_{N-L}]$ : a zero vector of size $(N - L)$ .
$h_{\theta}(\mathbf{x})$	<i>conditioning network</i> (data-dependent convolution kernel): $h_{\theta}(\mathbf{x}) = \text{NN}_{\theta}(\mathbf{x})$ that is a neural network parameterized by $\theta$ .
<code>Conv1d</code>	1D depthwise linear convolution with a short kernel length (typically 3-5) applied to each feature dimension
<code>FFN()</code>	feed forward networks
<code>MLP()</code>	Multi-Layer Perceptron which represents a dense linear layer $\text{MLP}(\mathbf{x}) = \mathbf{x}\mathbf{W}$
<code>PosEmb()</code>	a positional embedding of time step $t$
$h(t)$	positional encoding part of the convolution kernel: $h(t) = \text{FFN}(\text{PosEmb}(t))$

## B. Experimental Details

### B.1. Synthetic In-context Learning

We used associative recall task to evaluate in-context learning of the proposed model. Given a string of key-value tuples from a random dictionary, this task involves generating a value from a key. For instance, given the input  $([a, 1, b, e, \beta, f], b)$ , the model is expected to return  $e$ , the value associated with the key  $b$ . This task assesses whether a model can effectively retrieve the correct value from a key in a prompt, essentially applying a data-controlled shift. While attention mechanisms offer this capability by computing pair-wise attention scores and then weighting the entire sequence accordingly (Olsson et al., 2022), they face computational difficulties for very large sequence.

The model is composed of 2 Orchid block while each Orchid is composed of a chain of order 1.5, including 2 element-wise multiplications and one data-dependent convolution. The hidden size of all models in this experiments are set to 64. The conditioning network, defined in (2), was used which was composed of a 1D depthwise convolution (`Conv1d`) in the time domain and a `Conv1d` in the frequency domain that were applied separately to each feature dimension, both having a kernel of length 3.

For training, we used Adam optimizer (Kingma & Ba, 2014) with its standard settings ( $\beta_1 = .9, \beta_2 = .999$ ), and learning rate of 5e-4 with linear warmup schedule in 1000 steps. A weight decay of 0.1 was used as a regularizer. The Orchid models were trained Orchid on a single P100 GPU for small to medium sequence length and on a single V100 GPU for large sequences.

Table B.1: A summary of the Fine-tuning results on GLUE benchmark (Wang et al., 2018). Following the the methodology outlined in (Izsak et al., 2021), we use the standard evaluation metrics: Spearman’s correlation for STS-B, Matthew’s correlation for CoLA, F1 scores for QQP and MRPC, and accuracy for the other tasks. For MNLI, the average of multiclass accuracy (m) both multiclass accuracy of mismatched set (mm) is used.

Model	MNLI (m / mm)	RTE	QNLI	QQP	SST2	STS-B	CoLA	MRPC	Average
M2-BERT-base (80M)	78.4 / 78.6	68.5	84.6	86.7	92.0	86.3	53.0	89.8	79.9
Orchid-BERT-base (77M)	79.53 / 80.52	70.4	86.16	87.2	92.05	86.63	51.76	90.53	<b>80.6</b>
M2-BERT-large (260M)	81.7 / 81.9	72.8	84.7	87.8	93.3	88.0	59.2	90.0	82.2
Orchid-BERT-large (254M)	81.82 / 82.74	76.32	87.02	88.18	92.8	88.29	56.97	89.24	<b>82.65</b>

## B.2. Language Modeling

In our experiments, we replaced the attention layers in the standard BERT framework in (Devlin et al., 2018) with Orchid layers. For each Transformer block in the BERT-style model, we replaced the attention layers with Orchid layers for sequence mixing. Each Orchid layer was composed of a chain of order 1.5, including 2 element-wise multiplications and one data-dependent convolution. The conditioning network, defined in (2), was used which was composed of a short `Conv1d` in time domain and a `Conv1d` in the frequency domain that were applied separately to each feature dimension, both having a kernel of length 3. For dimension mixing, we also substituted the two dense matrices in the MLP layers with block-diagonal matrices of order 1 with  $b = 4$  blocks (Dao et al., 2022) and also add a residual long convolution to each Orchid layer, as in (Fu et al., 2023a).

Our BERT-style model, called Orchid-BERT-base, was composed of 12 layers with a hidden size of 768, the same dimension and depth as BERT-base resulting in Orchid-BERT-base having 77M parameters, compared to BERT-base’s 110M parameters. We also pre-trained Orchid-BERT-large of 254M parameters with hidden dimensions of 1536 and 12 layers.

For pre-training, we used decoupled Adam optimizer with  $\beta_1 = .9$ ,  $\beta_2 = .98$ , and learning rate of 8e-4 with linear warmup schedule within first 6% of the steps and then decay with linear rate. A weight decay of 1e-5 is used as a regularizer. Orchid models were pre-trained using masked language modeling with 30% masking over the C4 dataset (Raffel et al., 2019) with sequence length of 128 and the `bert-base-uncased` tokenizer. Models were pre-trained on a node of 4xA100 GPUs for 70k steps with batch size of 4096.

**Finetuning on GLUE Benchmark:** To evaluate the performance of Orchid-BERT models, we finetuned the pre-trained models on GLUE fine-tuning tasks, comparing them against the baseline models: BERT-base and BERT-large, and the recent long convolution-based models: M2-BERT-base and M2-BERT-large (Fu et al., 2023a). The fine-tuning process was executed in accordance with the methodology described by Izsak et al. (2021).

For all tasks, the sequence length was 128. For some of the tasks, we applied average pooling on the embeddings of all the non-padding tokens and use it as the model output. We followed (Izsak et al., 2021) in fine-tuning small dataset tasks: RTE, MRPC, and STS-B are initialized from the fine-tuned checkpoint of MNLI dataset. Models were fine-tuned on a node of 4xA100 GPUs.

In contrast to (Fu et al., 2023a), which performed a hyperparameter search for learning rate, weight decay, and number of epochs, we used the reported hyper-parameters in (Fu et al., 2023a) and didn’t perform a thorough search for them. As noted in (Izsak et al., 2021), hyperparameter search can result in substantial improvements in the performance. In particular for CoLA task, whose results are bellow M2-BERT, we anticipate that fine tuning the parameter will improve its performance. The detailed hyperparameters for each task is reported in Table B.2.

## B.3. Image Classification

We extended the application of Orchid to the Vision Transformer (ViT) architecture, introduced by Dosovitskiy et al. (2020), by replacing its attention mechanism with Orchid similar to language modeling task. The sinusoidal positional embeddings and global average-pooling were employed for the class token, following (Steiner et al., 2021; Beyer et al., 2022). We compared the performance of our model against recent long convolution-based models, specifically Hyena-ViT-b (Poli et al., 2023) and M2-ViT-b (Fu et al., 2023a). We evaluated the models on two widely used image classification datasets:

Table B.2: Hyperparameters for Orchid-bert-base (77M) and Orchid-BERT-large (254M) on Various GLUE Tasks. D-AdamW stands for Decoupled AdamW optimization algorithm. For QNLI task in Orchid-bert-base (77M) we applied average pooling.

Hyperparameter	MNLI	RTE	QNLI	QQP	SST2	STSB	CoLA	MRPC
<b>Orchid-bert-base (77M)</b>								
Optimizer	D-AdamW	AdamW	AdamW	AdamW	D-AdamW	AdamW	D-AdamW	AdamW
Learning Rate	5e-5	5e-5	5e-5	3e-5	3e-5	7e-5	5e-5	5e-5
Weight Decay	5e-6	0.01	1e-5	0.01	3e-6	0.01	5e-6	0.01
Epochs	3	6	10	10	3	10	10	10
<b>Orchid-bert-large (254M)</b>								
Optimizer	D-AdamW	D-AdamW	D-AdamW	D-AdamW	D-AdamW	D-AdamW	AdamW	D-AdamW
Learning Rate	5e-5	1e-5	5e-5	3e-5	3e-5	7e-5	5e-5	8e-5
Weight Decay	5e-6	1e-6	1e-5	3e-6	3e-6	3e-6	5e-6	8e-6
Epochs	3	3	10	5	3	10	10	10

CIFAR-10 and ImageNet-1K.

Each Orchid layer consists of a chain of order 1.5, involving 2 element-wise multiplications and one data-dependent convolution. The conditioning network (defined in Eq. 2) employs a combination of `Conv1d` layers in both the time and frequency domains, applied separately to each feature dimension with a kernel length of 3 and 5 for CIFAR-10 and ImageNet-1K, respectively.

**CIFAR-10:** For CIFAR-10, images were transformed into sequences of  $4 \times 4$  pixel patches and processed using a ViT architecture composed of 6 Transformer layers with a hidden size of 128. For training, we used Adam optimizer with its standard setting ( $\beta_1 = .9, \beta_2 = .999$ ), and learning rate of 3e-4 with linear warmup schedule within first 500 steps. A weight decay of 0.05 was used as a regularizer. Orchid was trained on a single P100 GPU for 500 epochs with batch size of 512.

**ImageNet-1K:** We segmented images into patches of  $16 \times 16$  pixels, and we trained a ViT-base architecture featuring 12 Transformer layers and a hidden size of 768. We incorporated a residual long convolution within each Orchid layer and substituted the dense matrices in the MLP layers responsible for feature mixing with block-diagonal matrices of order 1 with  $b = 4$  blocks, reducing their computational complexity and the total model’s size.

For training, we used Adam optimizer with its standard setting ( $\beta_1 = .9, \beta_2 = .999$ ), and base learning rate of 1e-3 with linear warmup schedule within first 10 epochs and then decay with Cosine schedule. For data augmentation, we adopted the T2T-ViT pipeline (Yuan et al., 2021), including Random erasing with rate=0.25, CutMix with  $\alpha=1.0$ , Mixup with  $\alpha=0.8$ , AugMix, and RandAugment with [magnitude=9, magnitude-std=0.5, layers=2]. We trained Orchid on 4xA100 GPUs for 300 epochs and batch size of 1024.

Table B.3 summarizes architecture and training settings.

Table B.3: Architecture and training settings for Orchid-ViT models.

	ImageNet-1k	CIFAR-10
Number of Orchid blocks	12	6
Hidden dimension	768	128
Short <code>Conv1d</code> kernel size	5	3
<code>PosEmb</code> dimension	33	5
Patch size	$16 \times 16$	$4 \times 4$
Batch size	1024	512
Training epochs	300	500
Weight decay	0.05	0.05
Learning rate schedule	Cosine decay with linear warmup	Constant with linear warmup
Base learning rate	1e-3	3e-4
Warmup	10 epochs	500 steps
Label smoothing	0.1	0.1